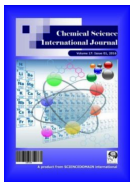

Chemical Science International Journal

22(4): 1-14, 2018; Article no.CSIJ.41452
ISSN: 2456-706X
(Past name: American Chemical Science Journal, Past ISSN: 2249-0205)

Chemical Reactivity Theory Applied to the Calculation of the Local Reactivity Descriptors of a Colored Maillard Reaction Product

Juan Frau[1] **and Daniel Glossman-Mitnik**[1,2*]

[1] *Departament de Química, Universitat de les Illes Balears, Palma de Mallorca, 07122, Spain.*
[2] *Laboratorio Virtual NANOCOSMOS, Departamento de Medio Ambiente y Energía, Centro de Investigación en Materiales Avanzados, Chihuahua, Chih 31136, Mexico.*

Authors' contributions

This work was carried out in collaboration between both authors. Author DGM designed the study, performed the calculations, and wrote the first draft of the manuscript. Author JF managed the analyses of the study and the literature searches. Both authors read and approved the final manuscript.

Article Information

DOI: 10.9734/CSJI/2018/41452
Editor(s):
(1) Francisco Marquez-Linares, Department of Chemistry, Nanomaterials Research Group, School of Science and Technology, University of Turabo, USA.
Reviewers:
(1) Nobuaki Tanaka , Shinshu University, Japan.
(2) Oyeneyin, Oluwatoba Emmanuel, Adekunle Ajasin University, Nigeria.
Complete Peer review History: http://www.sciencedomain.org/review-history/24626

Original Research Article

Received 9th February 2018
Accepted 10th May 2018
Published 15th May 2018

ABSTRACT

This computational study assessed ten density functionals that include CAM-B3LYP, LC-ωPBE, M11, M11L, MN12L, MN12SX, N12, N12SX, ωB97X, and ωB97XD related to the Def2TZVP basis set together with the SMD solvation model. These are assessed in calculating the molecular properties and structure of the pyrrolopyrrole-2-carbaldehyde molecule (PPA) in water. The chemical reactivity descriptors for the systems are calculated via the Conceptual Density Functional Theory. The choice of active sites applicable to nucleophilic, electrophilic as well as radical attacks is made by linking them with Fukui functions indices, electrophilic Parr functions, and condensed dual descriptor $\Delta \mathbf{f}(\mathbf{r})$.

**Corresponding author: E-mail: daniel.glossman@cimav.edu.mx;*

The predicted Maximum absorption wavelength tends to be considerably accurate relative to the experimental value. The study found the MN12SX and N12SX density functionals to be the most appropriate in predicting the chemical reactivity of this molecule.

Keywords: PPA; conceptual DFT; chemical reactivity theory; Parr function; maximum absorption wavelength.

1 INTRODUCTION

Visual color in processed foods is largely due to colored products of Maillard or nonenzymic browning reactions. In spite of the longstanding aesthetic and practical interest in Maillard derived food coloring materials, relatively little is known about the chemical structures responsible for visual color [1]. These chemical structures are known as Colored Maillard Reaction Products and can be isolated at intermediate stages during the melanoidins formation process.

Besides their interest as dye molecules which may be useful as food additives, but also as dyes for dye-sensitized solar cells (DSSC), these compounds have also antioxidant capabilities. Thus, they are amenable to be studied by analyzing their molecular reactivity properties.

One of these isolated molecules is called PPA (pyrrolopyrrole-2-carbaldehyde) [2] which has interesting properties as a colored compound and fluorescent dye and we believe that it could be of interest to study its molecular reactivity by using the ideas of Conceptual DFT, in the same way of our previous works [3, 4, 5, 6, 7, 8, 9, 10, 11, 12, 13, 14, 15].

Thus, in this computational study we will assess ten density functionals in calculating the molecular properties and structure of the PPA intermediate melanoidin pigment in water. Following the same ideas of previous works, we will consider fixed range-separated hybrid (RSH) density functionals instead of the optimally-tuned RSH density functionals that have attained great success [16, 17, 18, 19, 20, 21, 22, 23, 24, 25, 26, 27, 28, 29, 30, 31, 32, 33, 34, 35].

2 THEORETICAL BACKGROUND

The theoretical background of this study is similar to the previous conducted research presented [3, 4, 5, 6, 7, 8, 9, 10, 11, 12, 13, 14, 15], and will be shown here for complete purposes, because this research is a component of a major project that it is in progress.

If we consider the KID (Koopmans in DFT) procedure presented in our previous works together with a finite difference approximation, then the global reactivity descriptors can be written as:

Electronegativity	$\chi = -\frac{1}{2}(I + A) \approx \frac{1}{2}(\epsilon_L + \epsilon_H)$	[36]
Global Hardness	$\eta = (I - A) \approx (\epsilon_L - \epsilon_H)$	[36]
Electrophilicty	$\omega = \frac{\mu^2}{2\eta} = \frac{(I+A)^2}{4(I-A)} \approx \frac{(\epsilon_L+\epsilon_H)^2}{4(\epsilon_L-\epsilon_H)}$	[37]
Electrodonating Power	$\omega^- = \frac{(3I+A)^2}{16(I-A)} \approx \frac{(3\epsilon_H+\epsilon_L)^2}{16\eta}$	[38]
Electroaccepting Power	$\omega^+ = \frac{(I+3A)^2}{16(I-A)} \approx \frac{(\epsilon_H+3\epsilon_L)^2}{16\eta}$	[38]
Net electrophilicity	$\Delta\omega^{\pm} = \omega^+ - (-\omega^-) = \omega^+ + \omega^-$	[39]

where ϵ_H and ϵ_L are the energies of the highest occupied and the lowest unoccupied molecular orbitals (HOMO and LUMO), respectively.

Applying the same ideas, the definitions for the local reactivity descriptors are:

Nucleophilic Fukui Function	$f^{+}(\mathbf{r}) = \rho_{N+1}(\mathbf{r}) - \rho_{N}(\mathbf{r})$	[36]
Electrophilic Fukui Function	$f^{-}(\mathbf{r}) = \rho_{N}(\mathbf{r}) - \rho_{N-1}(\mathbf{r})$	[36]
Dual Descriptor	$\Delta f(\mathbf{r}) = \left(\frac{\partial f(\mathbf{r})}{\partial N}\right)_{v(\mathbf{r})}$	[40]
Nucleophilic Parr Function	$P^{-}(\mathbf{r}) = \rho_{s}^{rc}(\mathbf{r})$	[41]
Electrophilic Parr Function	$P^{+}(\mathbf{r}) = \rho_{s}^{ra}(\mathbf{r})$	[41]

where $\rho_{N+1}(\mathbf{r})$, $\rho_{N}(\mathbf{r})$, and $\rho_{N-1}(\mathbf{r})$ are the electronic densities at point $\mathbf{r}$ for the system with $N+1$, N, and $N-1$ electrons, respectively, and $\rho_{s}^{rc}(\mathbf{r})$ and $\rho_{s}^{ra}(\mathbf{r})$ are related to the atomic spin density (ASD) at the **r** atom of the radical cation or anion of a given molecule, respectively [42].

3 SETTINGS AND COMPUTATIONAL METHODS

Following the lines of our previous work , the computational studies were performed with the Gaussian 09 [43] series of programs with density functional methods as implemented in the computational package. The basis set used in this work was Def2SVP for geometry optimization and frequencies, while Def2TZVP was considered for the calculation of the electronic properties [44, 45]. All the calculations were performed in the presence of water as the solvent by doing Integral Equation Formalism-Polarized Continuum Model (IEF-PCM) computations according to the Solvation Model Density (SMD) solvation model [46].

For the calculation of the molecular structure and properties of the studied systems, we have chosen ten density functionals which are known to consistently provide satisfactory results for several structural and thermodynamic properties:

CAM-B3LYP	Long-range-corrected B3LYP by the CAM method	[47]
LC-ωPBE	Long-range-corrected ωPBE density functional	[48]
M11	Range-separated hybrid meta-GGA	[49]
M11L	Dual-range local meta-GGA	[50]
MN12L	Nonseparable local meta-NGA	[51]
MN12SX	Range-separated hybrid nonseparable meta-NGA	[52]
N12	Nonseparable local NGA	[53]
N12SX	Range-separated hybrid NGA	[52]
ωB97X	Long-range corrected density functional	[54]
ωB97XD	ωB97X version including empirical dispersion	[55]

In these functionals, GGA stands for generalized gradient approximation (in which the density functional depends on the up and down spin densities and their reduced gradient) and NGA stands for nonseparable gradient approximation (in which the density functional depends on the up/down spin densities and their reduced gradient, and also adopts a nonseparable form).

4 RESULTS AND DISCUSSION

The molecular structure of the PPA molecule was taken from PubChem (https://pubchem.ncbi.nlm.nih. gov), a website that acts as the public repository for information pertaining chemical substances together with the biological activities they are associated with.The

pre-optimization of the systems was done using random sampling that involved molecular mechanics techniques and inclusion of the various torsional angles via the general MMFF94 force field [56, 57, 58, 59, 60] through the Marvin View 17.15 program that constitutes an advanced chemical viewer suited to multiple and single chemical queries, structures and reactions (https://www.chemaxon. com). Afterwards, the structure that the resultant lower-energy conformer assumed for this molecule was reoptimized using the ten density functionals mentioned in the previous section together with the Def2SVP basis set as well as the SMD solvation model using water as the solvent.

The analysis of the results obtained in the study aimed at verifying that the KID procedure was fulfilled. On doing it previously, several descriptors associated with the results that HOMO and LUMO calculations obtained are related with results obtained using the vertical I and A following the ΔSCF procedure. A link exists between the three main descriptors and the simplest conformity to the Koopmans' theorem by linking ϵ_H with -I, ϵ_L with -A, and their behavior in describing the HOMO-LUMO gap as $J_I = |\epsilon_H + E_{gs}(N-1) - E_{gs}(N)|$, $J_A = |\epsilon_L + E_{gs}(N) - E_{gs}(N+1)|$, and $J_{HL} = \sqrt{{J_I}^2 + {J_A}^2}$. Notably, the J_A descriptor consists of an approximation that remains valid only when the HOMO that a radical anion has (the SOMO) shares similarity with the LUMO that the neutral system has. Consequently, we decided to design another descriptor ΔSL as the difference between the orbital energies of the SOMO and the LUMO, to guide in verifying how the approximation is accurate.

The results of the calculation of the electronic energies of the neutral, positive and negative molecular systems (in au) of PPA, the HOMO, LUMO and SOMO orbital energies (also in au), J_I, J_A, J_{HL} and ΔSL descriptors calculated with the ten density functionals and the Def2TZVP basis set using water as a solvent simulated with the SMD parametrization of the IEF-PCM model are presented in Table 1.

As presented in previous works [3, 4, 5, 6, 7, 8, 9, 10, 11, 12, 13, 14, 15], we consider four other descriptors that analyze how well the studied density functionals are useful for the prediction of the electronegativity χ, the global hardness η, and the global electrophilicity ω, and for a combination of these Conceptual DFT descriptors, considering only the energies of the HOMO and LUMO or the vertical I and A: $J_\chi = |\chi - \chi_K|$, $J_\eta = |\eta - \eta_K|$, $J_\omega = |\omega - \omega_K|$, and $J_{CDFT} = \sqrt{J_\chi^2 + J_\eta^2 + J_\omega^2}$, where CDFT stands for Conceptual DFT. The results of the calculations of J_χ, J_η, J_ω, and J_{CDFT} for the low-energy conformer of PPA in water are displayed in Table 2.

Table 1. Electronic energies of the neutral, positive, and negative molecular systems (in au) of PPA, the HOMO, LUMO, and SOMO orbital energies (in eV); and J_I, J_A, J_{HL}, and ΔSL descriptors calculated with the ten density functionals and the Def2TZVP basis set using water as solvent simulated with the SMD parametrization of the IEF-PCM mode

	Eo	E+	E-	HOMO	LUMO	SOMO	J(I)	J(A)	J(HL)	ΔSL
CAM-B3LYP	-1177.8455	-1177.6458	-1177.9149	-6.8584	-0.4076	-3.3574	1.4215	1.4786	2.0511	2.9497
LC-ωPBE	-1177.6339	-1177.4282	-1177.7105	-8.1186	0.4806	-4.6382	2.5217	2.5667	3.5982	5.1188
M11	-1177.7707	-1177.5627	-1177.8436	-7.9322	0.3382	-4.2962	2.2729	2.3243	3.2509	4.6344
M11L	-1177.7358	-1177.5232	-1177.8170	-5.4505	-2.5269	-1.8474	0.3375	0.3176	0.4634	0.6795
MN12L	-1177.2943	-1177.0926	-1177.3596	-5.1713	-2.0373	-1.4996	0.3162	0.2586	0.4085	0.5377
MN12SX	-1177.3580	-1177.1498	-1177.4294	-5.6214	-1.9192	-1.9639	0.0433	0.0255	0.0503	0.0446
N12	-1178.1808	-1177.9909	-1178.2420	-4.7626	-2.0711	-1.2482	0.4052	0.4063	0.5739	0.8229
N12SX	-1177.8289	-1177.6301	-1177.8973	-5.4121	-1.8128	-1.8942	0.0011	0.0476	0.0476	0.0814
ωB97X	-1178.0821	-1177.8802	-1178.1522	-7.8152	0.4544	-4.2657	2.3205	2.3635	3.3122	4.7201
ωB97XD	-1178.0049	-1177.8025	-1178.0750	-7.4807	0.1181	-3.9275	1.9741	2.0272	2.8296	4.0455

As Tables 1 and 2 provide, the KID procedure applies accurately from MN12SX and N12SX density functionals that are range-separated hybrid meta-NGA as well as range-separated hybrid NGA density functionals respectively. In fact, the values of J_I, J_A, and J_{HL} are actually not zero. Nevertheless, the results tend to be impressive especially for the MN12SX density functional. As well, the ΔSL descriptor reaches the minimum values when MN12SX and N12SX density functionals are used in the calculations. This implies that there are sufficient justifications to assume that the LUMO of the neutral approximates the electron affinity. The same density functionals follow the KID procedure in the rest of the descriptors such as J_χ, J_η, J_ω, and J_{CDFT}.

In the past, various TDDFT studies of molecules of different size have used optimally-tuned RSH density functionals with great success [16, 17, 18, 19, 20, 21, 22, 23, 24, 25, 26, 27, 28, 29, 30, 31, 32, 33, 34, 35]. The considerable success of the approach is however undermined by the issue of the tuning optimization being system dependent. Therefore, focus should be on establishing the effectiveness of the behaviors of the fixed RSH density functionals in describing the excitation characteristics. In his works, Becke has recently mentioned that the adiabatic connection and the ideas of Hohenberg, Kohn, and Sham apply only to electronic ground states is a common misconception [61]. Furthermore, consistent with Baerends et al., KS model is not appreciated for being superior because of its lowest excitation energy in molecules. Physically, it amounts to an excitation of the KS system rather than electron adittion as would be the case in Hartree-Fock. Thus, it can be effectively be used as a measure of the optical gap and is an effective approximation to the gap (in molecules) [62]. In their conclusion, van Meer et al. advanced that the HOMO-LUMO gap associated with the KS model tends to be an approximation of the lowest excitation energy, a desirable characteristic with no concerns regarding it [63].

In this work, the determination of the maximum absorption wavelength of the PPA molecule in water is performed by conducting ground state calculations with the mentioned ten density functionals obtaining the HOMO-LUMO gap which are compared with TDDFT calculations using the Def2TZVP basis set. Fig. 1 provide an illustration that compares graphically the results involved in the ground-state approximation derived from the HOMO-LUMO gap together with TDDFT results and the experimental value of 348 nm in water. A similar comparison is shown in Table 3.

Having verified that the MN12SX/Def2TZVP model chemistry is a good choice for the calculation of the global reactivity descriptors and the prediction of the Maximum absorption wavelength from the ground state calculation of the HOMO and LUMO, we now present the optimized molecular structure of PPA in water in Fig. 2. Meanwhile, the calculated bond lengths and bond angles are shown in Tables 4 and 5.

Table 2.J_χ, J_η, J_ω, and J_{CDFT} for the PPA molecule in water

	J_χ	J_η	J_ω	J_{CDFT}
CAM-B3LYP	0.0281	2.9053	0.8672	3.0321
LC-ωPBE	0.0217	5.0863	1.2515	5.2381
M11	0.0247	4.5943	1.1149	4.7278
M11L	0.0085	0.6518	0.4865	0.8134
MN12L	0.0282	0.5775	0.2950	0.6491
MN12SX	0.0337	0.0202	0.0238	0.0459
N12	0.0006	0.8104	0.5025	0.9536
N12SX	0.0228	0.0511	0.0494	0.0746
ωB97X	0.0202	4.6833	1.0903	4.8086
ωB97XD	0.0260	3.9990	1.0173	4.1264

Table 3. Maximum absorption wavelength (λ_{max}) of the PPA molecule calculated from the HOMO-LUMO gap and from TDDFT results in comparison with the experimental value

	λ_{max}(HL)	Δ(HL)	λ_{max}(TDDFT)	Δ(TDDFT)
CAM-B3LYP	192	45	303	13
LC-ωPBE	144	59	292	16
M11	150	57	306	12
M11L	424	22	352	1
MN12L	396	14	331	5
MN12SX	335	4	318	9
N12	461	32	379	9
N12SX	345	1	324	7
ωB97X	150	57	294	16
ωB97XD	163	53	301	14

Table 4. Calculated bond lengths (in Å) of the PPA molecule with the MN12SX density functional using water as the solvent simulated with the SMD solvation model

Bond	Distance	Bond	Distance	Bond	Distance	Bond	Distance
R(1-2)	1.393	R(7-28)	1.439	R(15-21)	1.441	R(28-35)	1.515
R(1-6)	1.387	R(8-9)	1.094	R(17-19)	1.122	R(31-32)	1.213
R(1-25)	1.438	R(8-10)	1.411	R(17-20)	1.117	R(31-33)	1.374
R(2-3)	1.389	R(10-11)	1.455	R(17-23)	1.439	R(33-34)	0.985
R(2-14)	1.501	R(11-12)	1.227	R(21-22)	0.984	R(35-36)	1.218
R(3-4)	1.093	R(11-13)	1.143	R(23-24)	0.980	R(35-37)	1.382
R(3-5)	1.424	R(14-15)	1.530	R(25-26)	1.109	R(37-38)	0.982
R(5-6)	1.406	R(14-16)	1.111	R(25-27)	1.114	R(12-30)	1.963
R(5-7)	1.370	R(14-39)	1.112	R(25-31)	1.537		
R(6-8)	1.407	R(15-17)	1.526	R(28-29)	1.117		
R(7-10)	1.392	R(15-18)	1.130	R(28-30)	1.116		

Table 5. Calculated bond angles (in) of the PPA molecule with the MN12SX density functional using water as the solvent simulated with the SMD solvation model

Bond	Angle	Bond	Angle	Bond	Angle	Bond	Angle
A(2-1-6)	108.0	A(3-5-7)	143.5	A(11-12-30)	102.9	A(26-25-27)	107.0
A(2-1-25)	126.4	A(6-5-7)	108.0	A(15-14-16)	108.8	A(26-25-31)	109.0
A(1-2-3)	110.0	A(5-6-8)	108.9	A(15-14-39)	108.7	A(27-25-31)	109.4
A(1-2-14)	120.8	A(5-7-10)	108.5	A(14-15-17)	113.1	A(25-31-32)	123.2
A(6-1-25)	125.6	A(5-7-28)	125.8	A(14-15-18)	107.9	A(25-31-33)	114.7
A(1-6-5)	107.6	A(6-8-9)	128.8	A(14-15-21)	109.4	A(29-28-30)	107.5
A(1-6-8)	143.5	A(6-8-10)	105.6	A(16-14-39)	106.1	A(29-28-35)	109.1
A(1-25-26)	108.4	A(10-7-28)	125.7	A(17-15-18)	108.5	A(30-28-35)	110.4
A(1-25-27)	110.8	A(7-10-8)	109.1	A(17-15-21)	109.0	A(28-30-12)	134.6
A(1-25-31)	112.1	A(7-10-11)	124.1	A(15-17-19)	110.6	A(28-35-36)	126.3
A(3-2-14)	129.2	A(7-28-29)	110.6	A(15-17-20)	111.2	A(28-35-37)	113.0
A(2-3-4)	125.4	A(7-28-30)	107.8	A(15-17-23)	107.3	A(32-31-33)	122.1
A(2-3-5)	105.8	A(7-28-35)	111.4	A(18-15-21)	108.9	A(31-33-34)	108.9
A(2-14-15)	113.9	A(9-8-10)	125.6	A(15-21-22)	105.4	A(36-35-37)	120.7
A(2-14-16)	109.4	A(8-10-11)	126.8	A(19-17-20)	107.5	A(35-37-38)	107.8
A(2-14-39)	109.6	A(10-11-12)	124.7	A(19-17-23)	110.3		
A(4-3-5)	128.8	A(10-11-13)	114.2	A(20-17-23)	109.9		
A(3-5-6)	108.6	A(12-11-13)	121.1	A(17-23-24)	107.8		

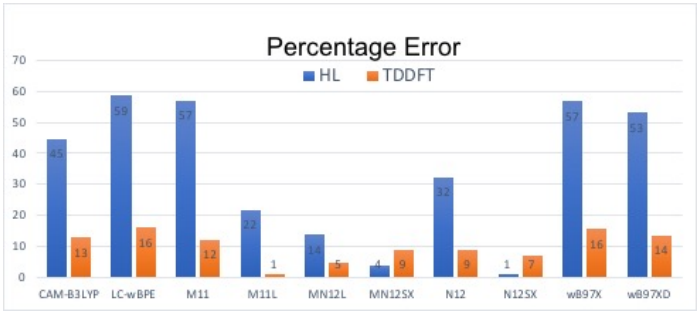

Fig. 1. A graphical comparison of the results for the calculation of the λ_{max} of the PPA molecule between the HOMO-LUMO gap prediction, TDDFT values, and experimental data

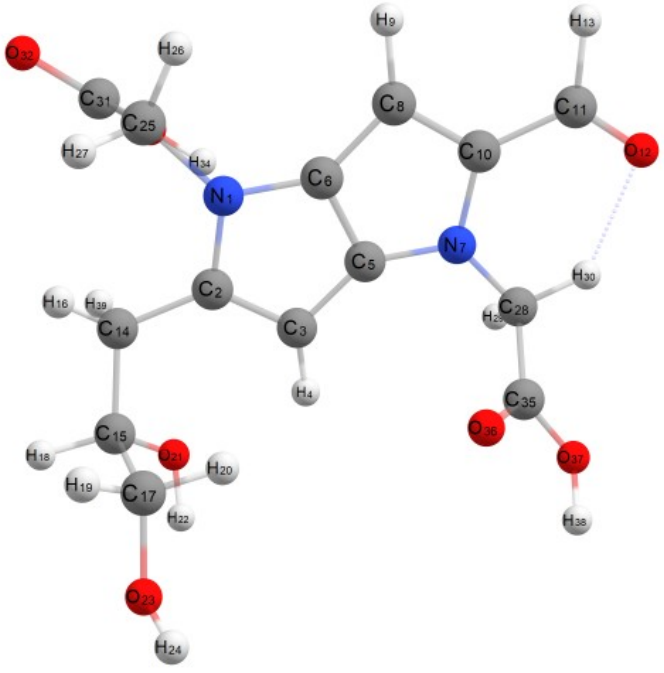

Fig. 2. A schematic representation of the optimized structure of the PPA molecule calculated with the MN12SX density functional showing the numbering of the atoms

Table 6. Global reactivity descriptors for the PPA molecule with the MN12SX density functional using water as the solvent simulated with the SMD solvation model

Electronegativity (χ)	Chemical Hardness (η)	Electrophilicity (ω)
3.7703	3.7021	1.9199
Electrodonating Power (ω^-)	Electroaccepting Power (ω^+)	Net Electrophilicity ($\Delta\omega^\pm$)
3.5024	2.1218	5.6242

As a summary of the previous results, the global reactivity descriptors for the PPA molecule calculated with the MN12SX/Def2TZVP model chemistry in water are presented in Table 6(above).

The calculations of the condensed Fukui functions and dual descriptor are done by using the Chemcraft molecular analysis program to extract the Mulliken and NPA atomic charges [64] beginning with single-point energy calculations involving the MN12SX density functional that uses the Def2TZVP basis set in line with the SMD solvation model, and water utilized as the solvent.

Considering the potential application the PPA molecule as an antioxidant, it is of interest to get insight into the active sites for radical attack. A graphical representation of the radical Fukui function f^0 (as an average of the nucleophilic and electrophilic Fukui functions) calculated with the MN12SX/Def2TZVP model chemistry in water is presented in Fig. 3.

The condensed electrophilic and nucleophilic Parr functions P_k^+ and P_k^- over the atoms of the PPA molecule in water have been calculated by extracting the Mulliken and Hirshfeld (or CM5) atomic charges using the Chemcraft molecular analysis program [64] starting from single-point energy calculations of the ionic species with the MN12SX density functional using the Def2TZVP basis set in the presence of the solvent according to the SMD solvation model.

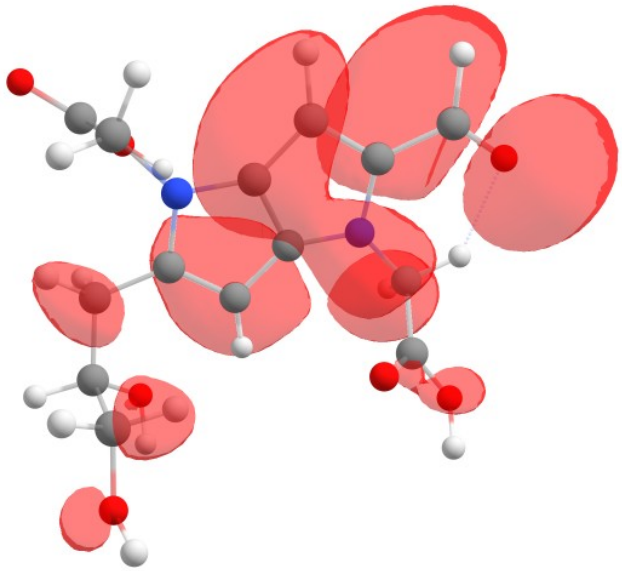

Fig. 3. A graphical representation of the radical Fukui function f^0 of the PPA molecule calculated with the MN12SX/Def2TZVP model chemistry in water

Table 7. The condensed dual descriptor calculated with Mulliken atomic charges Δf_k (M) and with NPA atomic charges Δf_k (N), electrophilic and nucleophilic Parr functions with Mulliken atomic spin densities P_k^+ (M) and P_k^- (M), and electrophilic and nucleophilic Parr functions with Hirshfeld (or CM5) atomic spin densities P_k^+ (H) and P_k^- (H) for the PPA molecule. Hydrogen atoms are not shown.

Atom	Δf_k (M)	Δf_k (N)	P_k^+ (M)	P_k^- (M)	P_k^+ (H)	P_k^- (H)
1N	-0.06	0.96	0.0081	-0.0285	0.0133	0.0139
2C	-8.48	-6.41	0.1829	0.3030	0.1033	0.2019
3C	-13.39	-9.84	-0.0590	0.1286	-0.0032	0.1209
5C	0.69	2.90	0.1035	0.0612	0.0610	0.0779
6C	-10.75	-9.90	-0.0617	0.1729	-0.0037	0.1196
7N	2.53	3.14	0.0759	0.0015	0.0576	0.0288
8C	12.01	11.86	0.2376	-0.0417	0.1494	0.0238
10C	-16.32	-17.01	-0.0311	0.3329	0.0445	0.2131
11C	26.10	22.92	0.3614	-0.0678	0.2786	0.0107
12O	9.22	4.69	0.2290	0.1300	0.2254	0.1090
14C	-0.45	-0.77	-0.0223	-0.0281	0.0105	0.0197
15C	-0.15	-0.15	0.0038	0.0026	0.0025	0.0045
17C	-0.41	-0.03	-0.0010	0.0090	0.0009	0.0070
21O	-0.09	-0.11	0.0005	0.0021	0.0003	0.0016
23O	-0.36	-0.44	0.0003	0.0043	0.0003	0.0044
25C	-0.04	-0.27	-0.0003	-0.0010	0.0010	0.0006
28C	0.03	-0.22	-0.0055	-0.0020	0.0049	0.0014
31C	-0.04	-0.01	0.0000	-0.0002	0.0004	0.0000
32O	-0.06	-0.41	0.0000	0.0002	0.0000	0.0002
33O	-0.03	-0.31	0.0005	0.0025	0.0005	0.0014
35C	0.16	-0.31	0.0031	0.0007	0.0031	0.0007
36O	0.02	-0.03	-0.0001	0.0000	0.0005	0.0003
37O	0.02	0.17	0.0005	0.0000	0.0009	0.0000

The results for the condensed dual descriptor calculated with Mulliken atomic charges Δf_k (M), with NPA atomic charges Δf_k (N), the electrophilic and nucleophilic Parr functions with Mulliken atomic spin densities P_k^+ (M) and P_k^- (M), and the electrophilic and nucleophilic Parr functions with Hirshfeld (or CM5) atomic spin densities P_k^+ (H) and P_k^- (H) are displayed in Table 7 for the PPA molecule in water.

From the results for the local reactivity descriptors in Table 7 (above), it can be concluded that C11 will be the preferred site for a nucleophilic attack and that this atom will act as an electrophilic species in a chemical reaction. In turn, it can be appreciated that C3 and C10 will be prone to electrophilic attacks and that these atomic sites will act as nucleophilic species in chemical reactions that involve the PPA molecule.

5 CONCLUSION

Ten fixed RSH density functionals, including CAM-B3LYP, LC-ωPBE, M11, N12, M11L, MN12L, N12SX, MN12SX, ωB97X and ωB97XD, were examined to determine whether they fulfill the empirical KID procedure. The assessment was conducted by comparing the values from HOMO and LUMO calculations to those generated by the ΔSCF technique for the PPA molecule in water. This is a compound which is of academic as well as industrial interest. The study has observed that the range-separated and hybrid meta-NGA density functionals tend to be the most suited in meeting this goal. Thus, they can be suitable alternatives to density functionals where the behavior of them are optimally tuned using a gap-fitting procedure. They also exhibit the desirable prospect of benefiting future studies aimed at understanding the chemical reactivity

of colored melanoidins with larger molecular weights when reducing sugars react with proteins and peptides.

From the results of this work, it becomes evident that it is easy to predict the sites of interaction of the PPA molecule under study. This involves having DFT-based reactivity descriptors, including Parr functions and dual descriptor calculations. Evidently, the descriptors are useful in characterizing and describing the preferred reactive sites. They are also useful in comprehensively explaining the reactivity of the molecules.

Furthermore, it is also possible to predict the Maximum absorption wavelength for the PPA in water with considerable accuracy. The prediction involves the MN12SX density functional, beginning with the HOMO-LUMO gap instead of TDDFT calculations. Such a finding is particularly crucial considering the likelihood of it being used to inform the alternative determination method on the color that larger systems such as prosthetic chromophore groups. This becomes necessary in circumstance when it is not possible to carry out TDDFT calculations.

Acknowledgment

This work has been partially supported by CIMAV, SC and Consejo Nacional de Ciencia y Tecnología (CONACYT, Mexico) through Grant 219566-2014 for Basic Science Research. Daniel Glossman-Mitnik conducted this work while a Visiting Lecturer at the University of the Balearic Islands from which support is gratefully acknowledged. This work was cofunded by the Ministerio de Economía y Competitividad (MINECO) and the European Fund for Regional Development (FEDER) (CTQ2014-55835-R).

COMPETING INTERESTS

Authors have declared that no competing interests exist.

References

[1] Rizzi GP. Chemical structure of colored maillard reaction products. Food Reviews International. 1997;13(1):1-28.

[2] Hayase F, Usui T, Ono Y, Shirahashi Y, Machida T, Ito T, Nishitani N, Shimohira K, Watanabe H. Formation mechanisms of melanoidins and fluorescent pyridinium compounds as advanced glycation end products. Annals of the New York Academy of Sciences. 2008;1126:53-58.

[3] Frau J, Mu F,ñoz, Glossman-Mitnik D. A Comparison of the minnesota family of density functionals for the calculation of conceptual dft descriptors: Citrus flavonoids as a test case. Research Journal of Chemical Sciences. 2017;7(5):46-58.

[4] Frau J, Glossman-Mitnik D. A Comparative study of the glycating power of simple carbohydrates in the maillard reaction by means of conceptual Dft descriptors. British Journal of Applied Science and Technology. 2017;21(1): 32795.

[5] Frau J, Mu F,ñoz, Glossman-Mitnik D. A conceptual dft study of the chemical reactivity of magnesium octaethylprphyrin (MgOEP) as Predicted by the minnesota family of density functional. Química Nova. 2017;40(4): 402-406.

[6] Frau J, Glossman-Mitnik D. Pyridoxamine derivatives as non enzymatic glycation inhibitors: The conceptual Dft viewpoint. Research Journal of Life Sciences, Bioinformatics, Pharmaceutical and Chemical Sciences. 2017;2(6):103-122.

[7] Frau J, Glossman-Mitnik D. Molecular modeling study of the structures, properties and glycating power of some reducing disaccharides. MOJ Drug Design Development Therapy. 2017;1(1):00003.

[8] Frau J, Glossman-Mitnik D. Computational prediction of the reactivity sites of alzheimer amyloid β-Peptides Aβ40 and Aβ42. ChemXpress. 2017;10(1):120.

[9] Frau J, Glossman-Mitnik D. Conceptual dft descriptors of amino acids with potential corrosion inhibition properties calculated with the latest minnesota density functional. Frontiers in Chemistry. 2017;5:16.

[10] Sastre S, Frau J, Glossman-Mitnik D. Computational prediction of the protonation sites of ac-lys-(ala)n-lys-NH2 peptides through conceptual dft and medt descriptors. Molecules. 2017;22(3):458.

[11] Frau J, Ramis R, Glossman-Mitnik D. Computational prediction of the preferred glycation sites of model helical peptides derived from human serum albumin (HSA) and lysozyme helix 4 (LH4). Theoretical Chemistry Accounts. 2017;136(4):39.

[12] Frau J, Mu F.ñoz, Glossman-Mitnik D. Application of dft concepts to the study of the chemical reactivity of some resveratrol derivatives through the assessment of the validity of the ?koopmans in Dft? (KID) procedure. Journal of Theoretical and Computational Chemistry. 2017;16(1):1750006.

[13] Frau J, Glossman-Mitnik D. Chemical reactivity theory study of advanced glycation endproduct inhibitors. Molecules. 2017;22(1):226.

[14] Frau J, Glossman-Mitnik D. A conceptual dft study of the molecular properties of glycating carbonyl compounds. Chemistry Central Journal. 2017;11: 8.

[15] Frau J, N,ández-Haro Hern, Glossman-Mitnik D. Computational prediction of the pKas of small peptides through conceptual dft descriptors. Chemical Physics Letters. 2017;671:138-141.

[16] Jacquemin D, Moore B, Planchat A, Adamo C, Autschbach J. Performance of an optimally tuned range-separated hybrid functional for 0-0 Electronic excitation energies. Journal of Chemical Theory and Computation. 2014;10(4):1677-1685.

[17] Egger DA, Weissman S, Refaely-Abramson S, Sharifzadeh S, Dauth M, Baer R, Kümmel S,. Neaton JB, Zojer E, Kronik L. Outer-valence electron spectra of prototypical aromatic heterocycles from an optimally tuned range-separated hybrid functional. Journal of Chemical Theory and Computation. 2014;10(5):1934-1952.

[18] Foster ME, Wong BM. Nonempirically tuned range-separated dft accurately predicts both fundamental and excitation gaps in DNA and RNA nucleobases. Journal of Chemical Theory and Computation. 2012;8(8):2682-2687.

[19] Foster ME, Azoulay JD, Wong BM, Allendorf MD. Novel metal–organic framework linkers for light harvesting applications. Chemical Science. 2014;5(5):2081-2090.

[20] Karolewski A, Stein T, Baer R, Kümmel S. Communication: Tailoring the optical gap in light-harvesting molecules. The Journal of Chemical Physics. 2011;134(15) :151101-5.

[21] Karolewski A, Kronik L, Kümmel S. Using optimally tuned range separated hybrid functionals in ground-state calculations: Consequences and caveats. The Journal of Chemical Physics. 2013;138(20):204115.

[22] Koppen JV, Hapka M, Szczeniak MM, Chalasinski G. Optical absorption spectra of gold clusters Au(n) (n = 4, 6, 8,12, 20) from long-range corrected functionals with optimal tuning. The Journal of Chemical Physics. 2012;137(11):114302.

[23] Kronik L, Stein T, Refaely-Abramson S, Baer R. Excitation gaps of finite-sized systems from optimally tuned range-separated hybrid functional. Journal of Chemical Theory and Computation. 2012;8(5):1515-1531.

[24] Kuritz N, Stein T, Baer R, Kronik L. Charge-transfer-like $\pi \rightarrow \pi^*$ excitations in time-dependent density functional theory: A conundrum and its solution. Journal of Chemical Theory and Computation. 2011;7(8):2408-2415.

[25] Lima IT, Prado AdS, Martins JBL, De Oliveira Neto PH, Ceschin AM, Da Cunha WF, Da Silva Filho DA. Improving the description of the optical properties of carotenoids by tuning the long-range corrected functionals. The Journal of Physical Chemistry A. 2016;120(27):4944-4950.

[26] Manna AK, Lee MH, McMahon KL, Dunietz BD. Calculating high energy charge transfer states using optimally tuned range-separated hybrid functional. Journal of Chemical Theory and Computation. 2015;11(3):1110-1117.

[27] Mooren II B, Autschbach J. Longest-wavelength electronic excitations of linear cyanines: The role of electron delocalization and of approximations in time-dependent density functional theory. Journal of Chemical Theory and Computation. 2013;9(11):4991-5003.

[28] Niskanen M, Hukka TI. Modeling of photoactive conjugated donor-acceptor copolymers: The effect of the exact hf exchange in dft functionals on geometries and gap energies of oligomer and periodic models. Phys. Chem. Chem. Phys. 2014;16(26):13294-13305.

[29] Pereira TL, Leal LA, Da Cunha WF, Timóteo de Sousa Júnior 0052, Ribeiro Junior LA, Antonio da Silva Filho D. Optimally tuned functionals improving the description of optical and electronic properties of the phthalocyanine molecule. Journal of Molecular Modeling. 2017;23(3):71.

[30] Phillips H, Zheng S, Hyla A, Laine R, Goodson III T, Geva E, Dunietz BD. Ab initio calculation of the electronic absorption of functionalized octahedral silsesquioxanes via time-dependent density functional theory with range-separated hybrid functional. The Journal of Physical Chemistry A. 2012;116(4):1137-1145.

[31] Phillips H, Geva E, Dunietz BD. Calculating off-site excitations in symmetric donor-acceptor systems via time-dependent density functional theory with range-separated density functionals. Journal of Chemical Theory and Computation. 2012;8(8):2661-2668.

[32] Refaely-Abramson S, Baer R, Kronik L. Fundamental and excitation gaps in molecules of relevance for organic photovoltaics from an optimally tuned range-separated hybrid functional. Physical Review B. 2011;84(7):075144-8.

[33] Stein T, Kronik L, Baer R. Prediction of charge-transfer excitations in coumarin-based dyes using a range-separated functional tuned from first principles. The Journal of Chemical Physics. 2009;131(24): 244119.

[34] Stein T, Kronik L, Baer R. Reliable prediction of charge transfer excitations in molecular complexes using time-dependent density functional theory. Journal of the American Chemical Society. 2009;131(8):2818-2820.

[35] Sun H, Autschbach J. Electronic energy gaps for π-conjugated oligomers and polymers calculated with density functional theory. Journal of Chemical Theory and Computation. 2014;10(3):1035-1047.

[36] Parr R, Yang W. Density functional approach to the frontier-electron theory of chemical reactivity. Journal of the American Chemical Society. 1984;106:4049-4050.

[37] Parr R, Szentpaly L, Liu S. Electrophilicity index. Journal of the American Chemical Societ. 1999;121:1922-1924.

[38] Gázquez J, Cedillo A, Vela A. Electrodonating and electroaccepting Powers. Journal of Physical Chemistry A. 2007;111(10):1966-1970.

[39] Chattaraj P, Chakraborty A, Giri S. Net electrophilicity. Journal of Physical Chemistry A. 2009;113(37):10068-10074.

[40] Morell C, Grand A, Toro-Labbé A. New dual descriptor for chemical Reactivity. Journal of Physical Chemistry A. 2005;109:205-212.

[41] Domingo LR, Pérez P, Sáez J. Understanding the local reactivity in polar organic reactions through electrophilic and nucleophilic parr functions. RSC Advances. 2013;3:1486-1494.

[42] Domingo LR, Ríos-Gutiérrez M, Pérez P. Applications of the conceptual density functional theory indices to organic chemistry reactivity. Molecules. 2016;21:748.

[43] Frisch MJ, Trucks GW,. Schlegel HB, Scuseria GE, Robb MA, Cheeseman JR, Scalmani G, Barone V, Mennucci B, Petersson GA, H. Nakatsuji, M. Caricato, X. Li, H. P. Hratchian, A. F. Izmaylov, J. Bloino, G. Zheng, J. L. Sonnenberg, M. Hada, M. Ehara, K. Toyota, R. Fukuda, J. Hasegawa, M. Ishida, T. Nakajima, Y. Honda, O. Kitao, H. Nakai, T. Vreven, J. A. Montgomery, Jr., J. E. Peralta, F. Ogliaro, M. Bearpark, J. J. Heyd, E. Brothers, K. N. Kudin, V. N. Staroverov, R. Kobayashi, J. Normand, K. Raghavachari, A. Rendell, J. C. Burant, S. S. Iyengar, J. Tomasi, M. Cossi, N. Rega, J. M. Millam, M. Klene, J. E. Knox, J. B. Cross, V. Bakken, C. Adamo, J. Jaramillo, R. Gomperts, R. E. Stratmann, O. Yazyev, A. J. Austin, R. Cammi, C. Pomelli, J. W. Ochterski, R. L.

Martin, K. Morokuma, V. G. Zakrzewski, G. A. Voth, P. Salvador, J. J. Dannenberg, S. Dapprich, A. D. Daniels, O. Farkas, J. B. Foresman, J. V. Ortiz, J. Cioslowski, D. J. Fox, Gaussian 09 Revision D.01, Gaussian Inc., Wallingford CT, 2009 (2018).

[44] Weigend F, Ahlrichs R. Balanced basis sets of split valence. Triple zeta valence and quadruple zeta valence quality for H to Rn: Design and assessment of accuracy. Physical Chemistry Chemical Physics. 2005;7: 3297-3305.

[45] Weigend F. Accurate coulomb-fitting basis sets for H to R. Physical Chemistry Chemical Physics. 2006;8:1057-1065.

[46] Marenich A, Cramer C, Truhlar D. Universal solvation model based on solute electron density and a continuum model of the solvent defined by the bulk dielectric constant and atomic surface tensions. Journal of Physical Chemistry. 2009;B 113: 6378-6396.

[47] Yanai T, Tew DP, Handy NC. A New hybrid exchange-correlation functional using the coulomb-attenuating method (CAM-B3LYP). Chemical Physics Letters. 2004;393(1-3):51-57.

[48] Henderson TM, Izmaylov AF, Scalmani G, Scuseria GE. Can short-range hybrids describe long-range-dependent properties? The Journal of Chemical Physics. 2009;131(4):044108.

[49] Peverati R, Truhlar DG. Improving the accuracy of hybrid meta-gga density functionals by range separation. The Journal of Physical Chemistry Letters. 2011;2(21):2810-2817.

[50] Peverati R, Truhlar DG. M11-l: A local density functional that provides improved accuracy for electronic structure calculations in chemistry and physics. The Journal of Physical Chemistry Letters. 2012;3(1):117-124.

[51] Peverati R,. Truhlar DG. An improved and broadly accurate local approximation to the exchange-correlation density functional: The MN12-L functional for electronic structure calculations in chemistry and physics. Physical Chemistry Chemical Physics. 2012;14(38):13171-13174.

[52] Peverati R, Truhlar DG. Screened-exchange density functionals with broad accuracy for chemistry and solid-state physics. Physical Chemistry Chemical Physics. 2012;14(47):16187-16191.

[53] Peverati R, Truhlar DG. Exchange-correlation functional with good accuracy for both structural and energetic properties while depending only on the density and its gradient. Journal of Chemical Theory and Computation. 2012;8(7) 2310-2319.

[54] Chai J, Head-Gordon M. Systematic optimization of long-range corrected hybrid density functionals. Journal of Chemical Physics. 2008;128:084106.

[55] Chai J, Head-Gordon M. Long-range corrected hybrid density functionals with damped atom-atom dispersion corrections. Physical Chemistry Chemical Physics. 2008;10:6615-6620.

[56] Halgren TA. Merck molecular force Field. I. basis, form, scope, parameterization, and performance of MMFF94. Journal of Computational Chemistry. 1996;17(5-6):490-519.

[57] Halgren TA. Merck molecular force field. II. MMFF94 van der waals and electrostatic parameters for intermolecular interactions. Journal of Computational Chemistry. 1996;17(5-6):520-552.

[58] Halgren TA. MMFF VI. MMFF94s option for energy minimization studies. Journal of Computational Chemistry. 1999;20(7):720-729.

[59] Halgren TA, Nachbar RB. Merck molecular force field. IV. conformational energies and geometries for MMFF94. Journal of Computational Chemistry 1996;17(5-6):587-615.

[60] Halgren TA. Merck molecular force field. V. extension of MMFF94 using experimental data, additional computational data, and empirical rules. Journal of Computational Chemistry. 1996;17(5-6):616-641.

[61] Becke AD. Vertical excitation energies from the adiabatic connection. The Journal of Chemical Physics. 2016;145(19):194107.

[62] Baerends EJ, Gritsenko OV, van Meer R. The Kohn-Sham gap, the fundamental gap and the optical gap: The physical meaning of occupied and virtual Kohn-Sham orbital energies. Physical Chemistry Chemical Physics 2013;15(39):16408-16425.

[63] van Meer R, Gritsenko OV, Baerends EJ. Physical meaning of virtual Kohn-Sham orbitals and orbital energies: An ideal basis for the description of molecular excitations. Journal of Chemical Theory and Computation. 2014;10(10) :4432-4441.

[64] Zhurko G, Zhurko D. Chemcraft program Revision 1.6, Grigoriy A. Zhurko, United States (2012).
URL http://www.chemcraft.com/

Peer-review history:
The peer review history for this paper can be accessed here:
http://www.sciencedomain.org/review-history/24626